Mechanisms of detachment in fibrillar adhesive systems

Pranav Sudersan[a], Michael Kappl[a,*]

[a] *Max Planck Institute for Polymer Research, Ackermannweg 10, 55128 Mainz, Germany*

Abstract

Several creatures can climb on smooth surfaces with the help of hairy adhesive pads on their legs. A rapid change from strong attachment to effortless detachment of the leg is enabled by the asymmetric geometry of the hairs. In this study, we propose mechanisms by which a hairy pad can be easily detached, even when the hairs possess no asymmetry. Here, we examine the possible function of the leg joint and the claws. Based on a spring-based model, we consider three modes of detachment: vertically pulling the pad while maintaining either a 1) fixed or a 2) free leg joint, or by 3) flexing the pad about the claw. We show that in all cases, the adhesion force can be significantly reduced due to elastic forces when the hairs deform non-uniformly across the array, an effect that we call "*elastic weakening*". Our proposed model illustrates the design advantage provided by such fibrillar adhesive systems, which not only provides strong adhesion, but also allows easy detachment, making it suitable as organs for fast locomotion. The presented approaches can be potentially used to switch the adhesion state in bio-inspired fibrillar adhesives, by incorporating artificial joints and claws into their design, without the need of asymmetric or stimuli-responsive fibrillar structures.

Keywords: fibrillar adhesion, reversible adhesion, contact splitting, beetle, biomechanics

*Corresponding author
Email address: kappl@mpip-mainz.mpg.de (Michael Kappl)

1. Introduction

Over the past few decades, there have been numerous studies to understand how animals such as geckos and insects are able to walk on surfaces of any direction while defying gravity. A microscopic observation reveals that, in many cases, animals have a dense array of fibrillar structures at the end of their legs [1, 2]. These "hairy" adhesive pads help the animal to stay attached to any surface or detach easily at will for countless cycles, a property that is referred to as *reversible adhesion*. Previous attempts to theoretically explain adhesion in hairy pads [3, 4] has followed two fundamental approaches: either by energy balance, or by force balance.

In the energy balance approach, adhesion is usually characterized by "work of adhesion" (W_{adh}), which is the energy required to separate a pad from the surface. During detachment, the elastic energy stored in the hair is dissipated, which increases W_{adh} and thus adhesion is enhanced [5, 6]. Detachment of an individual hair can be explained based on Kendall's peeling theory [7, 8], which predicts low forces at high peeling angles.

In the force balance approach, adhesion is characterized by pull-off force, F_p (or stress, σ_p), which is the minimum force necessary to separate two surfaces from contact. Based on a "cohesive zone model", Hui et. al. [9] had identified two regimes of single hair detachment: 1) a *flaw sensitive* regime, where, for large hair raidus, contact failure occurs due to crack propagation, initiated by a stress singularity at the edge of the hair, leading to low σ_p; 2) a *flaw insensitive* regime, where, for small hair raidus, the contact interface fails simultaneously, leading to high σ_p. Tian et. al. [10] had shown that the "spatula" shaped hair tips in a gecko's toe allows it to change adhesion by three orders of magnitude by laterally sliding and controlling the pulling angle to disorient the hairs. Federle [11] had further argued that the curved shape of the hair helps the pad to stay attached when pulled proximally, and easily detached by elastic recoil when pushed distally.

The theories presented so far suggests that low detachment force of a fibrillar

adhesive pad can be attained by 1) increasing the stress concentration by peeling the pad at high angles, or 2) laterally shearing the pad before pull-off, which requires the hairs to have an asymmetric geometry or curvature. However, some insects like male dock beetles predominantly possess flat "mushroom" tipped hairs on their pads [12], which are relatively less asymmetric compared to the "spatula" tipped hairs. This begs the question of how the beetle can still easily detach their legs during locomotion, since these mushroom shaped hairs should be resilient to detachment via lateral shearing. Artificial micro-pillar adhesives mimicking the mushroom shaped hairs of the beetle have in fact demonstrated its superior adhesive strength in comparison to other geometries [13, 14]. Introducing asymmetry into the pillar geometry of such mimics for easy detachment is however challenging due to current limitations in fabrication techniques and difficulty in scaling-up for practical applications [14]. Alternate strategies are thus desired to switch the adhesion state of symmetric pillar arrays in a reversible manner, e.g. by buckling the pillars under compressive load leading to their contact loss [15] or by using special materials reacting to external stimuli such as magnetic field [16], UV light [17] or temperature [18].

In this work, we propose the possible mechanisms by which adhesive pads with symmetric hairs can be easily detached under a theoretical framework. The hairy pad is modelled as an array of springs and the force-balance approach is used to quantify the net adhesion [19, 20]. We hope our work to provide strategies to control the adhesion force of an artificial micro-pillar adhesive, which has applications in bio-inspired climbing robots, pick-and-place operations and reusable adhesives.

2. Model

The fibrillar adhesive pad is assumed to be a one dimensional array of N_t hairs, each behaving like a spring with spring constant, k_h, and natural length, $l_{h,0}$ (Figure 1). The array backing is assumed to be stiff. The pad is attached to a linearly deformable leg, assumed to be another spring with spring constant,

k_l, and natural length, $l_{l,0}$. The leg is hinged to the array at a distance, s, from the right end of the array. The hinge is at a vertical distance, d_s, from the surface. The hairs are spaced apart by a width, w, and the array is of length, $L = (N_t - 1)\, w$. The pad is oriented at an instantaneous angle, θ, while making contact with a flat smooth surface. Each hair can attain a maximum length, $l_{h,p}$, before pull-off, such that its pull-off force, $f_p = k_h\,(l_{h,p} - l_{h,0})$. F_{net} is the net force on the pad and M_{net} is the the net torque about the hinge, at a particular instant during the detachment process.

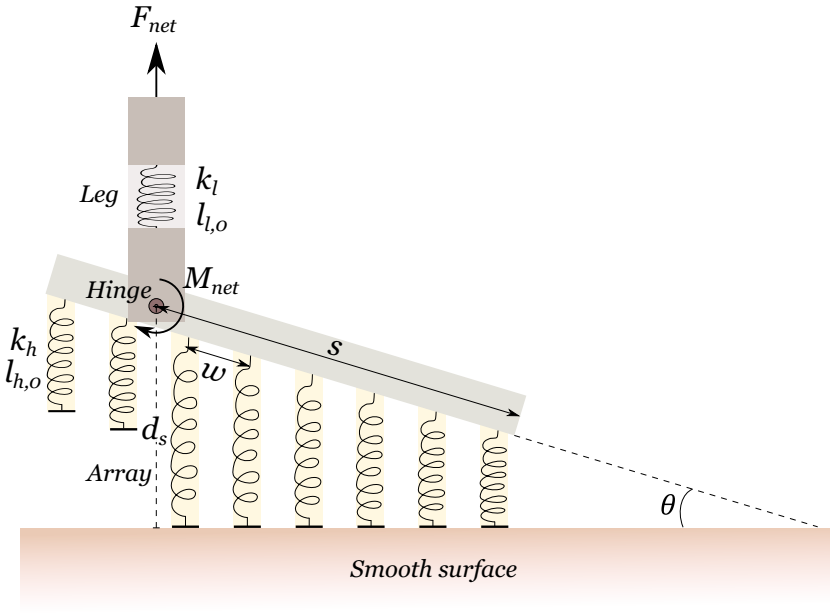

Figure 1: Spring contact model of a fibrillar adhesive pad. The pad consists of an array of N_t hairs connected to a deformable leg at the hinge. At a particular distance, d_s, n number of hairs are in contact and the array is oriented at a tilt angle, θ, with the surface.

Suppose at a particular instant, there are n hairs in contact with the surface. The net force on the whole pad will be,

$$F_{net} = \sum_{i=1}^{n} k_h\,(l_{h,i} - l_{h,0})$$

Simplifying, we get (see Appendix for derivation):

$$F_{net} = nk_h \left[d_s - l_{h,0} - \Psi \sin\theta \right] \tag{1}$$

where, $\Psi = s - \frac{n-1}{2} w$. For a particular value of n, equation 1 is valid until a certain distance, $d_{s,max}$, above which the left most hair will detach. Just before detachment, this hair will be at its maximum length, $l_{h,p}$. From simple geometry we can thus find:

$$d_{s,max} = l_{h,0} + \frac{f_p}{k_h} + \left[s - (n-1)\, w \right] \sin\theta \tag{2}$$

Equation 1 will be valid for $d_s \leq d_{s,max}$.

The maximum possible adhesion of the array would be the case when all hairs detach simultaneously ($\theta = 0°$):

$$F_{max} = N_t f_p \tag{3}$$

The net torque, M_{net}, about the hinge can be similarly derived (see Appendix):

$$M_{net} = nk_h \cos\theta \left[\left(d_s - l_{h,0} \right) \Psi - \left\{ \Psi^2 + \frac{n^2 - 1}{12} w^2 \right\} \sin\theta \right] \tag{4}$$

Let us now consider the scenario where even the leg above the hinge can undergo elastic stretching together with the hairs. When a hair detaches from the surface, the leg undergoes an elastic recoil due to the stored elastic energy. Suppose the leg relaxes upward by a recoil length, Δl. For n hairs in contact, the force balance before and after a hair detaches is given respectively by:

$$\sum_{i=1}^{n} k_h \left(l_{h,i} - l_{h,0} \right) = k_l \left(l_l - l_{l,0} \right)$$
$$\sum_{i=1}^{n-1} k_h \left(l_{h,i} + \Delta l - l_{h,0} \right) = k_l \left(l_l - \Delta l - l_{l,0} \right)$$

Solving the above two equations for Δl, we get:

$$\Delta l = \frac{f_p}{k_h \left(n - 1 \right) + k_l} \tag{5}$$

Thus, d_s shifts by Δl in equations 1 and 4 at each event of hair detachment (i.e. when $d_s = d_{s,max}$).

We express the forces and distances in non-dimensional forms, as below:

$$\hat{f}_p = \frac{f_p}{k_h w}, \quad \hat{F}_{net} = \frac{F_{net}}{k_h w}, \quad \hat{d}_s = \frac{d_s - l_{h,0}}{w}, \quad \hat{s} = \frac{s}{w}$$

Here, $\hat{f}_p$ is a parameter which encapsulates the hair's adhesion force, stiffness and array density. Unless specified, positive force values represent attraction by convention.

3. Detachment mechanisms

We consider three possible mechanisms to detach the adhesive pad from a surface: 1) *Fixed pull*, where the pad is pulled vertically up while keeping a fixed leg-hinge, 2) *Free pull,* where the pad is pulled vertically up while keeping the leg-hinge free to allow rotation of the array and 3) *Flex*, where the pad is hinged to an external point (claw-hinge), and detached in a rotary fashion, emulating the claw function in insects. To investigate each case in detail, let us assume a pad with $N_t = 25$ hairs and $\hat{f}_p = 0.1$ attached to a stiff leg ($k_l \to \infty$). The situation of a soft leg ($k_l/k_h = 10$) is also considered for the first two cases involving vertical detachment.

3.1. *Fixed pull*

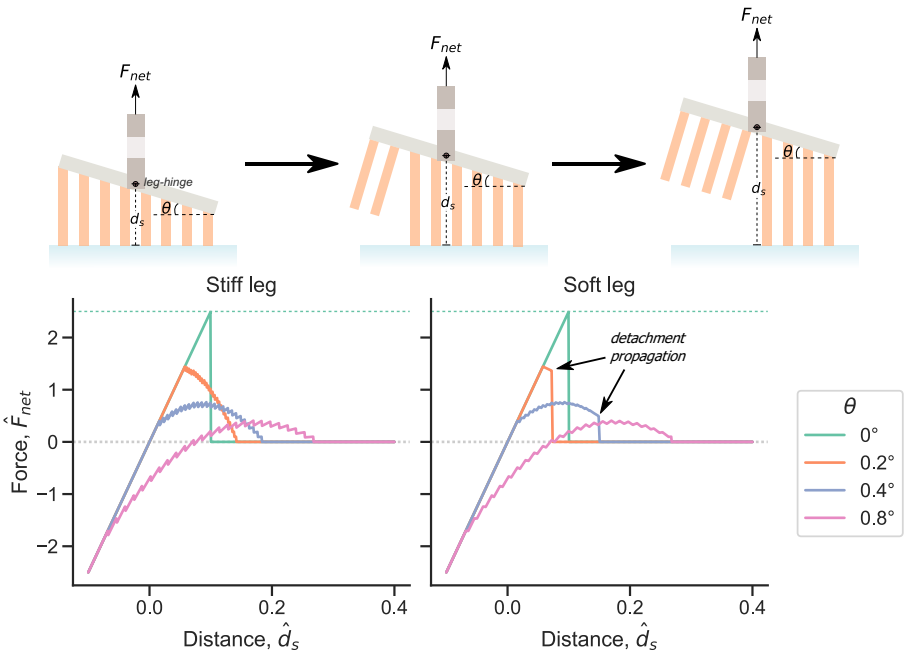

Figure 2: Force distance curves for a fibrillar adhesive pad, pulled vertically upwards with a fixed hinge between the pad and the leg (*Fixed pull*). The tilt angle, θ, of the array is kept fixed during detachment. The leg is either stiff ($k_l \to \infty$) or soft ($k_l/k_h = 10$). Positive force values represent attraction. The green dashed line represents the maximum possible adhesion for the pad. All values are normalized to dimensionless forms, as described in text.

The fibrillar adhesive pad can be detached by pulling it vertically upwards while maintaining a constant tilt angle, θ, with the surface. This can be achieved if the joint connecting the leg to the array (leg-hinge) is kept fixed. Equations 1, 2 and 3 can be used to get the resulting force-distance curves.

Increasing the tilt of the pad decreases its maximum force or adhesion (Figure 2). Tilting the pad causes an inhomogeneous deformation of hairs, where, on one end they are stretched, while, on the other end they are compressed. The balance of the respective attractive and repulsive elastic forces of the hairs ultimately results in a decrease in the net force. The tilted orientation also causes the individual hairs to detach distinctly rather than simultaneously, fur-

ther reducing the net adhesive power of the array. We term this effect of loss in adhesion due to a non-uniform hair deformation across the array as "*elastic weakening*". When there is no tilt ($\theta = 0°$), all the hairs undergo identical deformation and ultimately detaches simultaneously after a distance, $\hat{d}_s = 0.1$. Here, no *elastic weakening* occurs and the pad shows the maximum possible adhesion.

For the case of a stiff leg, we see that at small distances, all hairs of the pad are in contact with the surface, resulting in a linear force response. On further pulling, the hairs will start to detach sequentially from left to right, indicated by a characteristic "saw-tooth" jitter in the force curves. The hairs of the pad with a higher tilt angle will start to detach first, followed by the ones with a lower tilt.

For the case of a soft leg, we observe a similar effect of tilt angle on the force curves as before. The maximum adhesion force at a particular tilt is the same as that for the stiff leg. The saw-tooth jitter are however minimized due to the leg's deformation, leading to a "dampened" force response. Interestingly, the force abruptly drops to zero for the angles 0.2° and 0.4°. This is an effect of the elastic recoil of the leg while each hair loses contact during the detachment process (equation 5). The length difference between the detached hair just before it breaks contact and its adjacent hair is $w \sin\theta$. If the leg's recoil length, $\Delta l > w \sin\theta$, the adjacent hair will be stretched more than its maximum length ($l_{h,p}$), and thus will also detach, leading to further recoil of the leg. Equation 5 shows that Δl increases with every subsequent loss of hair contact if θ is kept constant. This implies that, once initiated, the leg's recoil will always be large enough to detach every remaining hair, resulting in a spontaneous propagation of the detachment front until the pad completely breaks contact with the surface. This is consistent with a recent report of catastrophic failure, due to a similar recoil effect of the measurement system, seen in micro-fibrillar adhesives with a narrow variance of individual fibril adhesive strengths [21].

3.2. Free pull

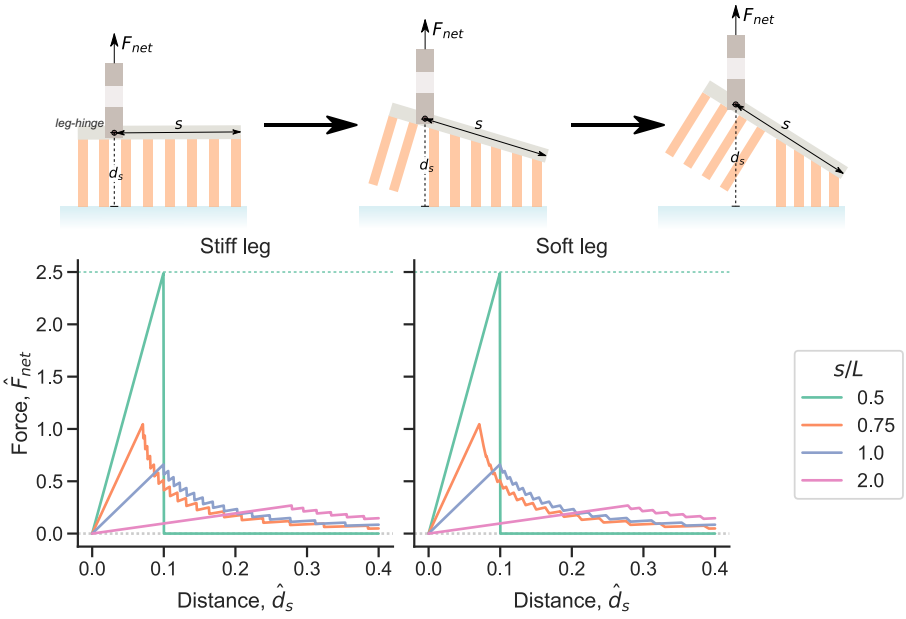

Figure 3: Force distance curves for a fibrillar adhesive pad, pulled vertically upwards with a free hinge between the pad and the leg (*Free pull*). s is the distance between the leg-hinge and the right end of the array and L is the array length. The free hinge allows further tilting of the array during the vertical pull. The leg is either stiff ($k_l \to \infty$) or soft ($k_l/k_h = 10$). Positive force values represent attraction. The green dashed line represents the maximum possible adhesion for the pad. All values are normalized to dimensionless forms, as described in text.

Similar to the previous case, we once again consider the situation where the adhesive pad is pulled vertically upwards for detachment. However now, the leg-hinge is assumed to be free. In this case, the array will reorient itself to maintain a zero net torque about the leg-hinge during the entire detachment process. At any given instant, the tilt angle, θ, can be found by setting M_{net} to zero in equation 4 to get:

$$\theta\left(\hat{d}_s, n\right) = \arcsin\left[\frac{\left(\hat{s} - \frac{n-1}{2}\right)\hat{d}_s}{\left(\hat{s} - \frac{n-1}{2}\right)^2 + \frac{n^2-1}{12}}\right] \tag{6}$$

Using the above relation together with equations 1, 2 and 3, we can find force-distance curves during a free vertical pull of the adhesive pad. Since the position of the leg-hinge will influence the net torque, we use the ratio, s/L, to study its effect on the detachment forces.

Maximum adhesion is seen when the leg-hinge is positioned at the centre of the array, i.e. $s/L = 0.5$ (Figure 3). Here, the net torque due to the hairs is balanced by symmetry and the array remains parallel to the substrate until all hairs detach simultaneously at $\hat{d_s} = 0.1$. Shifting the position of the leg-hinge further away from the array centre leads to lower forces or adhesion. The resulting torque imbalance will tilt the array, which reduces the net force due to the *elastic weakening* effect, as described in the previous section. Higher s/L increases the net torque to be balanced, leading to a higher tilt of the array and thus lower net force.

The force curves look qualitatively different compared to the previous case of *fixed pull*. A sharp maxima is seen, coinciding with the point when the first hair detaches. Beyond this, the force starts to decrease sharply and once again shows the characteristic saw-tooth jitter as the subsequent hairs detach in sequence. Nearly identical trend is seen for both a stiff and a soft leg. The elastic recoil of the leg does slightly reduce the amplitude of the jitter for the soft leg case. However, no abrupt drop in the force is seen like before. As the hairs detach, the array gets tilted more and more, making it less likely for the recoil length, Δl, to exceed $w \sin\theta$ and detach the next adjacent hair. Thus here, we don't see any propagation of the detachment front when the leg is soft.

3.3. Flex

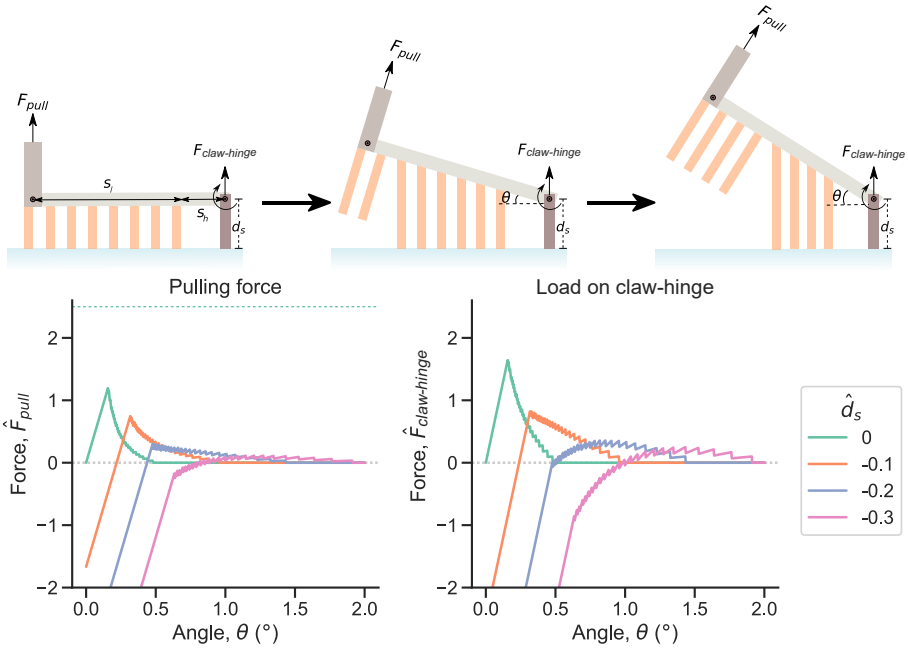

Figure 4: Force curves for a fibrillar adhesive pad detached by flexing it about the claw. $\hat{F}_{pull} = \frac{F_{pull}}{k_h w}$ is the normalised pulling force necessary to apply the torque about the claw-hinge for detachment, $\hat{F}_{hinge} = \frac{F_{hinge}}{k_h w}$ is the normalised reaction force on the claw-hinge, $\hat{d}_s = \frac{d_s - l_{h,0}}{w}$ is the normalized vertical distance of the claw-hinge from the surface. Here, $s_l/L = 1$ and $s_h/w = 10$. The green dashed line represents the maximum possible adhesion for the pad.

Instead of a vertical pull, the adhesive pad can also be detached by rotating it about the claw-hinge, located outside the array. Such a mode of detachment will be driven by a torque applied by the leg to rotate the pad around the claw-hinge until all the hairs lose contact. Let s_h be the distance between the claw-hinge and the right end of the array; s_l be the distance between the fixed leg-hinge and the right end of the array. To illustrate the mechanism, let us fix $s_l/L = 1$ and $s_h/w = 10$ and vary the vertical claw-hinge distance, d_s. At any particular instant, the pulling force applied by the leg, $F_{pull} = M_{net}/(s_l + s_h)$, where M_{net} is obtained by setting $s = -s_h$ in equation 4. Equation 1 will give

us the reaction force acting on the claw-hinge, $F_{claw-hinge}$.

Decreasing the vertical claw-hinge distance reduces the pulling force necessary to undergo detachment by flexing (Figure 4). One can imagine that initially, when the array is parallel to the surface, a lower value of d_s means the hairs are in a more compressed state. When the pad is subsequently rotated around the claw-hinge, the tilted array will once again lead to an *elastic weakening* effect due to the inhomogeneous deformation of hairs. This results in a decrease in the net torque and thus lower F_{pull} for smaller values of d_s. F_{pull} can be further reduced of course by increasing the lever arm $(s_l + s_h)$.

Detachment by flexing requires that the claw remains fixed and stable during the process. We see that generally, the normal load, acting on the hinge, $F_{claw-hinge}$, follows a similar trend as F_{pull} (Figure 4). For low values of d_s, $F_{claw-hinge}$ goes to negative values, implying that the claw should adhere well with the surface to resist this negative load. As the detachment progresses however, the array starts to exert a positive load on the claw.

4. Discussion

In order to characterize how a particular detachment mechanism influences the adhesion of the pad, we introduce a parameter, *reduction factor*, defined as:

$$r = \frac{N_t f_p}{F_{adh}} \tag{7}$$

Here, F_{adh} is the adhesion force required to detach the pad from the surface following a given mechanism and $N_t f_p$ is the maximum possible adhesion of the pad (equation 3). Reduction factor, r, represents the extent to which the adhesion can be reduced by choosing the mode of detachment. A large value of r implies that adhesion can be reduced by a greater factor, and this mode is more suitable to easily detach.

Effect of $\hat{f}_p$:. The dimensionless parameter, $\hat{f}_p = \frac{f_p}{k_h w}$, governs the strength and compliance of the array, where, high values represent a dense array of strongly

adhering soft hairs. Let us consider the case of an adhesive pad with $N_t = 25$ hairs and look at how $\hat{f}_p$ influences the reduction factor under each mode of detachment (Figure 5). From the heat maps, one can generally say that lower values of $\hat{f}_p$ increase the reduction factor and thus provide a greater possibility of controlling adhesion.

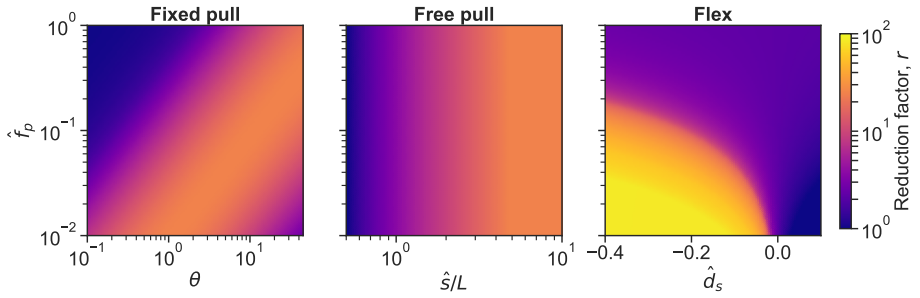

Figure 5: Heat maps showing the effect of the dimensionless parameter, $\hat{f}_p$, on the reduction factor for each mode of detachment. Here, we fix the number of hairs, $N_t = 25$. All values are normalized to dimensionless forms, as described in text.

When detachment follows the *fixed pull* method (Figure 5), for a constant $\hat{f}_p$, the reduction factor increases with increasing tilt angle, θ, and then decreases, showing a maximum r of 25 at an intermediate θ. Higher values of $\hat{f}_p$ shifts this maximum point to higher values of θ. This trend relates to the *elastic weakening* effect discussed before. Smaller values of θ bring a proportion of hairs under compression, reducing the adhesion and thus increasing r. On further tilting the array, eventually the proportion of stretched hairs will overcome the ones under compression, which ultimately reduces r at high θ. When the individual hairs show strong adhesion (i.e. for high $\hat{f}_p$), a greater tilt is necessary to bring the net adhesion of the array down.

For the case of detachment via *free pull*, $\hat{f}_p$ has no influence on the reduction factor. On the other hand, shifting the position of the leg-hinge further away from the array (i.e. high s/L) results in large values of r. In this scenario, the higher torque exerted by the array leads to a higher tilt, and thus increases the reduction factor via *elastic weakening*, saturating to the maximum value of 25.

For detachment by *flexing*, the reduction factor increases for higher initial compression of hairs (low $\hat{d}_s$). The pad notably shows a much higher reduction factor at low values of $\hat{f}_p$ and $\hat{d}_s$, with values as high as 100. Since this mode of detachment is driven by torque, the pulling force necessary to provide the torque can be decreased without any limit simply by having a long lever arm ($\hat{s}_l$). In contrast, for the previous cases of *free pull* and *fixed pull*, the reduction factor is capped to the maximum number of hairs in the array ($N_t = 25$). Here, *elastic weakening* can only reduce the array's adhesion force from N_t hairs down to a single hair at most.

Effect of N_t:. Let us now fix $\hat{f}_p = 0.1$ and investigate the influence of the number of hairs, N_t, on the reduction factor (Figure 6). The heat maps show that high N_t increases r irrespective of the mode of detachment. Under a tilted state, more number of hairs are compressed when N_t is high, which reduces the net adhesion. This highlights the advantage of having a split contact design found in many biological systems. Higher number of hairs offer a better control over adhesion and thus is more suited for reversible attachment and detachment during locomotion. The specific trends of reduction factor for each mode of detachment can be understood by similar arguments of *elastic weakening*, as discussed in the previous section.

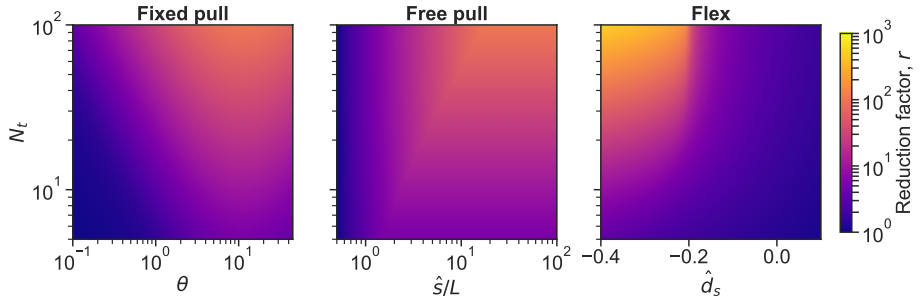

Figure 6: Heat maps showing the effect of the number of hairs, N_t, on the reduction factor for each mode of detachment. Here, we fix the dimensionless parameter, $\hat{f}_p = 0.1$. All values are normalized to dimensionless forms, as described in text.

Detachment pathways:. Based on the three modes of detachment discussed in the previous sections, one can think of several strategies to detach a fibrillar adhesive pad from the surface. To illustrate this, let us consider the adhesive system of a dock beetle. The beetle is known to have 3 sets of hairy pads in each of their legs, each possessing hairs of different geometries. To keep our analysis simple, we will assume each leg to have only two pads, with identical hairs of "mushroom" geometry. The distal and proximal pads possess roughly 500 and 1000 hairs, respectively [12]. Assuming the pads to be rectangular arrays of 20×25 and 40×25 hairs, we can model this as a one-dimensional system of 20 and 40 hairs, respectively, by combining the hairs along the width. Based on reported measurements [22], the beetle's "combined hair" is thus considered to have an effective pull-off force, $f_p = 0.5 \times 25 = 12.5$ μN and spring constant, $k_h = 0.5 \times 25 = 12.5$ N m^{-1}. The beetle's hairs are approximately $l_{h,0} = 40$ μm long, spaced $w = 10$ μm apart. The adhesive pad also has a claw, around 200 μm long, and the leg is connected roughly at the end of the proximal pad. This will put $\hat{s}_h = 20$ and $s_l/L = 1$, measured relative to the right end of the distal pad. The beetle's leg is assumed to possess two joints which could serve as a hinges for rotation (H_1 and H_2 in Figure 7 inset). The claw can be used as an external hinge (H_3) by flexing the pad around it.

Based on the above assumptions, we can come up with force-distance curves to detach the beetle's leg via various pathways (Figure 7). First, let us assume the hinge H_2 to be fixed, such that both the distal and proximal pads are combined to be a single long pad with $N_t = 60$ hairs. Path 1 shows the case where the pad shows maximum possible adhesion. Here, the combined pad is vertically pulled upwards while keeping the array perfectly parallel to the surface. If the pad is detached by keeping H_1 fixed and maintaining a tilt of 1° with the surface (path 2), the forces dramatically reduces, with around 10 times reduction in the adhesion compared to path 1. We can also detach the pad by switching between the different mechanisms. Path 3 shows one such example, where, initially the leg is pulled vertically up while keeping H_1 fixed, stretching the hairs. On reaching point a, H_1 is set free, which results in a sudden drop in

force due to the excess torque by the stretched hairs, tilting the array. Beyond this, the force curve follows the free pull mechanism, with ~ 3.5 times reduction in adhesion. An alternate strategy of switching between mechanisms would be to first apply a load on the pad (path 4) and compress the hairs until point b. Beyond this point, the claw can be used as a hinge to detach the pad via flexing it around H_3, which once again reduces the adhesion force. Now, if we assume the hinge H_2 to be free such that the two pads can behave distinctly, we can consider the scenario where the proximal pad is flexed around the distal pad at H_2 while keeping H_1 fixed (path 5). After the proximal pad has completely detached, H_1 can be freed up at point c to detach the distal pad via *free pull* with very little force. This pathway results in a ~ 5 times reduction in adhesion.

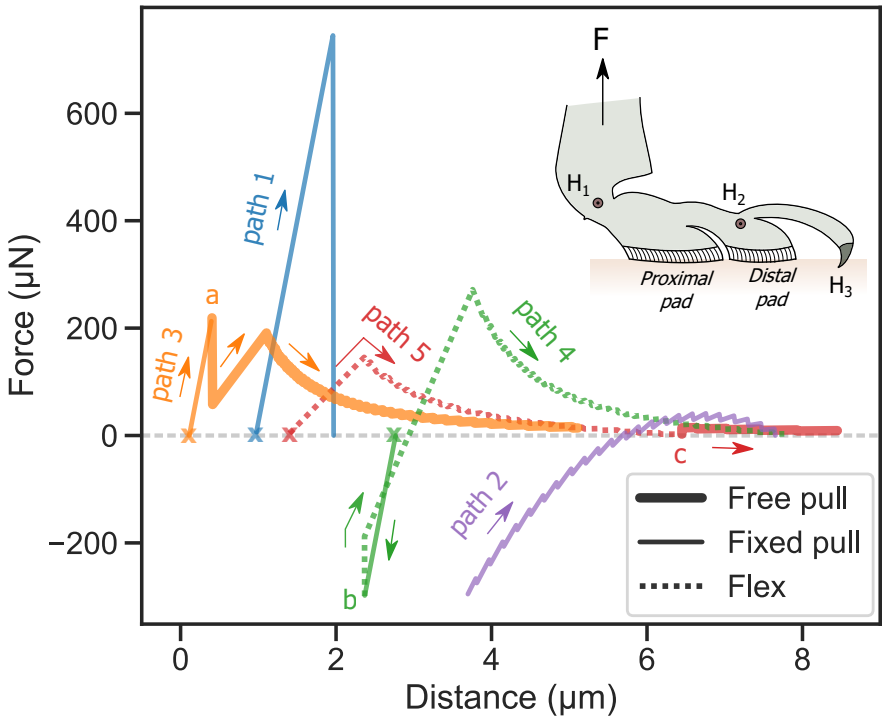

Figure 7: Force distance curves showing possible detachment pathways for a dock beetle's leg, derived from the spring contact model. The curves are offset laterally for clarity. Colours represent the distinct detachment pathways, as labelled correspondingly, with arrows indicating the direction of retraction. The different line style denotes the specific detachment mechanism followed by any region of the pathway. The inset schematic shows the assumed locations of the different hinges (H_1, H_2 and H_3) employed by the leg.

The above analysis illustrates how the design of the beetle's hairy adhesive pads is suitable for modulating its adhesion. Effective control and release of its leg joints can help the insect to reduce the pad's adhesion, allowing it to detach with little effort. High reduction in adhesion is seen when the pad is tilted relative to the surface during detachment, as a result of *elastic weakening*. To the best of our knowledge, there is no direct experimental evidence that beetles can modulate its adhesion by taking advantage of this effect. Considering that hair deformation occurs at length scales below 10 μm, direct observation of this

effect on running beetles would be challenging. A recent study on PDMS micropillar arrays, however, does indeed show a strong reduction in the adhesion force due to slight misalignments with the surface [23]. Based on previously reported microscopic investigation of freely walking dock beetles [24], we argue that the following experimental observations provide support to our proposed theory: 1) The detachment was shown to follow a three-dimensional twist of the leg, which suggests a complex inhomogeneous deformation of hairs across the array, leading to *elastic weakening*. 2) The beetle can at times instantaneously detach all its legs and "drop" itself while upside down. This could be explained by the beetle freeing up its leg joints and using just its body weight to provide the necessary force to detach all its legs via *free pull* (similar to path 3 above). 3) Only a fraction of the beetle's pads made contact with the surface during locomotion, which indicates that the pads should naturally be in a slightly tilted state. This not only reduces the contact area, but also non-uniformly deforms the hairs, both leading to a reduction in adhesion for easy detachment. 4) Contact images showed that the array "peels" from the proximal to distal direction during detachment. However, the beetle's hairs are attached to a relatively stiff backing [25], so it wouldn't be able to "peel" its array, since peeling, strictly speaking, depends on the elastic contribution of a thin flexible backing as it bends during the process [7]. Rather, the "peeling" observed in the beetle's case should be a result of the pad detaching from the surface in a tilted orientation, causing the hairs to detach in sequence. 5) The time scale of detachment was reported to be an order of magnitude shorter than the attachment time scale, which could be a result of the elastic recoil of the leg causing a spontaneous propagation of the detachment front (Figure 2).

There exists a limit to how much the pad can tilt, depending on its geometry and material properties. Suppose the hair has a maximum linear elastic strain limit, ε_m, and natural length, $l_{h,0}$. Based on Figure 1, if the right most hair is compressed to its elastic limit, we can show from simple geometry, that, the

corresponding maximum limit in tilt angle is given by:

$$\theta_{limit} = \arctan \frac{l_{h,0}\varepsilon_m}{(N_t - 1)\, w}$$

θ_{limit} will limit the reduction factor for each of the detachment mechanisms presented. Longer hairs can result in a lateral collapse or bundling of hairs, imposing an additional constraint on θ_{limit}. Large deformation of hairs can also lead to buckling, which will further limit the reduction in adhesion due to the smaller effective modulus. Thus, the geometry of the individual hairs is also crucial in effectively reducing adhesion by *elastic weakening*. Ideally, hairs with large diameters would be preferable to eliminate buckling, and optimally long hairs would provide a large range of angles to which the pad can be tilted while avoiding bundling.

5. Conclusion

Inhomogeneous deformation of hairs results in significant reductions in the adhesion of a fibrillar system. Such a condition can be achieved by either 1) pulling the pad while maintaining a constant tilt angle, 2) pulling the pad while maintaining a free leg joint or 3) flexing the pad around the claw. Strategic control of the joint's mobility or claw can allow the leg to easily switch between the above mechanisms, thus providing a simple way to reduce adhesion as per necessity. The presence of a deformable leg can further trigger a spontaneous propagation of hair detachment due to the leg's elastic recoil, making it suitable for fast detachment. Arrays with low $\hat{f}_p$ and large number of hairs, with a hair geometry that allows for large deformations while avoiding buckling and lateral bundling represent the optimal design conditions to maximize the range of control over adhesion. The proposed theory is supported by previously reported experimental observations of leg detachment in dock beetles and highlights possible role of the leg joint and claws to enable reversible adhesion. Similar strategies could potentially be adopted in the design of bio-inspired artificial fibrillar adhesives to easily switch the adhesion state without the need of asymmetric structures.

6. Acknowledgment

We are grateful to Prof. Dr. Hans-Jürgen Butt and Dr. Thomas Endlein (Max Planck Institute for Polymer Research, Germany) for reviewing the text, and thank Dr. Renè Hensel (Leibniz Institute for New Materials, Germany) and Dr. Bat-El Pinchasik (Tel-Aviv University, Israel) for fruitful discussions. This work was supported by the Deutsche Forschungsgemeinschaft [Grant number: PI 1351/2-1] and the Max Planck Graduate Center with the Johannes Gutenberg-Universität Mainz [MPGC].

Appendix A. Derivations

Suppose at a particular instant (Figure 1), there are n hairs in contact with the surface. The centre of the region of the array in contact is at a vertical distance, d', from the surface. The net force on the whole array is,

$$F_{net} = \sum_{i=1}^{n} k_h \left(l_{h,i} - l_{h,0} \right)$$

$l_{h,i}$ is the length of the i^{th} hair, which is at a horizontal distance, x_i, from the centre of the contact region. By simple geometry, $l_{h,i} = d' - x_i \tan\theta$. Substituting $l_{h,i}$ in above and noting that $\sum_{i=1}^{n} x_i = 0$ by symmetry, we get:

$$F_{net} = n k_h \left(d' - l_{h,0} \right)$$

From geometry, d_s and d' is related as:

$$\frac{d_s}{\sin\theta} - \frac{d'}{\sin\theta} = s - \frac{(n-1)\, w}{2}$$

Substituting for d', the net force, F_{net}, on the pad as a function of distance, d_s, is:

$$F_{net} = n k_h \left[d_s - l_{h,0} - \left[s - \frac{(n-1)\, w}{2} \right] \sin\theta \right]$$

The above equation is valid for $d_s \leq d_{s,max}$ at a particular value of n. We can get $d_{s,max}$ by considering the situation just before the left most hair is about

to detach (Figure 1). This hair will be at its maximum length, $l_{h,p}$. Once again from geometry, we see that $d_{s,max}$ and $l_{h,p}$ is related as:

$$\frac{l_{h,p}}{\sin\theta} - \frac{d_{s,max}}{\sin\theta} = (n-1)\,w - s$$

Substituting $l_{h,p} = \frac{f_p}{k_h} + l_{h,0}$ in above and simplifying, we get:

$$d_{s,max} = l_{h,0} + \frac{f_p}{k_h} + [s - (n-1)\,w]\sin\theta$$

The net torque about the hinge due to the deformed hairs of the array is,

$$M_{net} = \sum_{i=1}^{n} \lambda_i k_h \left(l_{h,i} - l_{h,0}\right)\cos\theta$$

Here, $\lambda_i = s - \left(\frac{n-1}{2}w - \frac{x_i}{\cos\theta}\right)$ is the length of the lever arm between the i^{th} hair and the hinge.

Substituting for $l_{h,i}$ and eliminating d' as before, we get:

$$M_{net} = \sum_{i=1}^{n} k_h \cos\theta \left[s - \left(\frac{n-1}{2}w - \frac{x_i}{\cos\theta}\right)\right]\left[d_s - \left(s - \frac{(n-1)\,w}{2}\right)\sin\theta - x_i\tan\theta - l_{h,0}\right]$$

To calculate $\sum_{i=1}^{n} x_i^2$, we follow:

$$\sum_{i=1}^{n} x_i^2 = 2\sum_{i=1}^{\frac{n}{2}} x_i^2 = 2\sum_{i=1}^{\frac{n}{2}}\left[w\cos\theta\left(i - \frac{1}{2}\right)^2\right] = 2w^2\cos^2\theta\left[\sum_{i=1}^{\frac{n}{2}} i^2 - \sum_{i=1}^{\frac{n}{2}} i - \sum_{i=1}^{\frac{n}{2}}\frac{1}{4}\right]$$

Using the identities $\sum_{i=1}^{N} i^2 = \frac{N(N+1)}{2}$ and $\sum_{i=1}^{N} i^2 = \frac{N(N+1)(2N+1)}{6}$ and simplifying, we get $\sum_{i=1}^{n} x_i^2 = n\left(\frac{n^2-1}{12}\right)w^2\cos^2\theta$. This, together with $\sum_{i=1}^{n} x_i = 0$ (by symmetry), the expression for M_{net} above can be simplified to finally get:

$$M_{net} = nk_h\cos\theta\left[\left(d_s - l_{h,0}\right)\left[s - \frac{(n-1)\,w}{2}\right] - \left\{\left[s - \frac{(n-1)\,w}{2}\right]^2 + \frac{n^2-1}{12}w^2\right\}\sin\theta\right]$$

References

[1] R. Hooke, Micrographia, or, Some physiological descriptions of minute bodies made by magnifying glasses : with observations and inquiries thereupon, The Royal Society, 1665.

[2] N. E. Stork, Experimental analysis of adhesion of *Chrysolina Polita* (chrysomelidae: Coleoptera) on a variety of surfaces, The Journal of Experimental Biology 88 (1) (1980) 91.

[3] D. Labonte, W. Federle, Scaling and biomechanics of surface attachment in climbing animals, Philos Trans R Soc Lond B Biol Sci 370 (1661) (2015) 20140027. doi:10.1098/rstb.2014.0027.

[4] R. D. O'Rorke, T. W. J. Steele, H. K. Taylor, Bioinspired fibrillar adhesives: a review of analytical models and experimental evidence for adhesion enhancement by surface patterns, Journal of Adhesion Science and Technology 30 (4) (2016) 362–391. doi:10.1080/01694243.2015.1101183.

[5] B. N. J. Persson, On the mechanism of adhesion in biological systems, The Journal of Chemical Physics 118 (16). doi:10.1063/1.1562192.

[6] A. Jagota, J. B. Stephen, Mechanics of adhesion through a fibrillar microstructure, Integrative and Comparative Biology 42 (6) (2002) 1140–1145.

[7] K. Kendall, Thin-film peeling-the elastic term, Journal of Physics D: Applied Physics 8 (13) (1975) 1449–1452. doi:10.1088/0022-3727/8/13/005.

[8] T. Endlein, A. Ji, D. Samuel, N. Yao, Z. Wang, W. J. P. Barnes, W. Federle, M. Kappl, Z. Dai, Sticking like sticky tape: tree frogs use friction forces to enhance attachment on overhanging surfaces, Journal of The Royal Society Interface 10 (80) (2013) 20120838. doi:10.1098/rsif.2012.0838.

[9] C. Y. Hui, N. J. Glassmaker, T. Tang, A. Jagota, Design of biomimetic fibrillar interfaces: 2. mechanics of enhanced adhesion, J R Soc Interface 1 (1) (2004) 35–48. doi:10.1098/rsif.2004.0005.

[10] Y. Tian, N. Pesika, H. Zeng, K. Rosenberg, B. Zhao, P. McGuiggan, K. Autumn, J. Israelachvili, Adhesion and friction in gecko toe attachment and detachment, Proceedings of the National Academy of Sciences

of the United States of America 103 (51) (2006) 19320–19325. doi:10.1073/pnas.0608841103.

[11] W. Federle, Why are so many adhesive pads hairy?, J Exp Biol 209 (Pt 14) (2006) 2611–21. doi:10.1242/jeb.02323.

[12] J. M. Bullock, W. Federle, Division of labour and sex differences between fibrillar, tarsal adhesive pads in beetles: effective elastic modulus and attachment performance, J Exp Biol 212 (Pt 12) (2009) 1876–88. doi:10.1242/jeb.030551.

[13] G. Carbone, E. Pierro, S. N. Gorb, Origin of the superior adhesive performance of mushroom-shaped microstructured surfaces, Soft Matter 7 (12) (2011) 5545–5552. doi:10.1039/C0SM01482F.

[14] A. del Campo, C. Greiner, E. Arzt, Contact shape controls adhesion of bioinspired fibrillar surfaces, Langmuir 23 (20) (2007) 10235–43. doi:10.1021/la7010502.

[15] D. Paretkar, M. Kamperman, D. Martina, J. Zhao, C. Creton, A. Lindner, A. Jagota, R. McMeeking, E. Arzt, Preload-responsive adhesion: effects of aspect ratio, tip shape and alignment, Journal of The Royal Society Interface 10 (83) (2013) 20130171. doi:10.1098/rsif.2013.0171.

[16] D.-M. Drotlef, P. Blümler, A. del Campo, Magnetically actuated patterns for bioinspired reversible adhesion (dry and wet), Advanced Materials 26 (5) (2014) 775–779. doi:10.1002/adma.201303087.

[17] E. Kizilkan, J. Strueben, A. Staubitz, S. N. Gorb, Bioinspired photocontrollable microstructured transport device, Science Robotics 2 (2) (2017) eaak9454. doi:10.1126/scirobotics.aak9454.

[18] J. Cui, D.-M. Drotlef, I. Larraza, J. P. Fernández-Blázquez, L. F. Boesel, C. Ohm, M. Mezger, R. Zentel, A. del Campo, Bioinspired actuated adhesive patterns of liquid crystalline elastomers, Advanced Materials 24 (34) (2012) 4601–4604. doi:https://doi.org/10.1002/adma.201200895.

[19] M. Schargott, V. L. Popov, S. Gorb, Spring model of biological attachment pads, Journal of Theoretical Biology 243 (1) (2006) 48–53. doi:https://doi.org/10.1016/j.jtbi.2006.05.023.

[20] M. Bacca, J. A. Booth, K. L. Turner, R. M. McMeeking, Load sharing in bioinspired fibrillar adhesives with backing layer interactions and interfacial misalignment, Journal of the Mechanics and Physics of Solids 96 (2016) 428–444. doi:https://doi.org/10.1016/j.jmps.2016.04.008.

[21] R. Hensel, J. Thiemecke, J. A. Booth, Preventing catastrophic failure of microfibrillar adhesives in compliant systems based on statistical analysis of adhesive strength, ACS Applied Materials & Interfacesdoi:10.1021/acsami.1c00978.

[22] J. M. Bullock, W. Federle, Beetle adhesive hairs differ in stiffness and stickiness: in vivo adhesion measurements on individual setae, Naturwissenschaften 98 (5) (2011) 381–7. doi:10.1007/s00114-011-0781-4.

[23] J. A. Booth, M. Bacca, R. M. McMeeking, K. L. Foster, Benefit of backing-layer compliance in fibrillar adhesive patches-resistance to peel propagation in the presence of interfacial misalignment, Advanced Materials Interfaces 5 (15) (2018) 1800272. doi:https://doi.org/10.1002/admi.201800272.

[24] S. M. Gernay, S. Labousse, P. Lambert, P. Compere, T. Gilet, Multi-scale tarsal adhesion kinematics of freely-walking dock beetles, J R Soc Interface 14 (136). doi:10.1098/rsif.2017.0493.

[25] H. Peisker, J. Michels, S. N. Gorb, Evidence for a material gradient in the adhesive tarsal setae of the ladybird beetle *Coccinella septempunctata*, Nat Commun 4 (2013) 1661. doi:10.1038/ncomms2576.